Journal of Medicinal Chemistry

Article

pubs.acs.org/jmc

SAR156497, an Exquisitely Selective Inhibitor of Aurora Kinases

Jean-Christophe Carry,*[,†] François Clerc,[†] Hervé Minoux,[‡] Laurent Schio,[†] Jacques Mauger,[#] Anil Nair,[#] Eric Parmantier,[†] Ronan Le Moigne,[†,∞] Cécile Delorme,[†] Jean-Paul Nicolas,[†] Alain Krick,[§] Pierre-Yves Abécassis,[§] Véronique Crocq-Stuerga,[∥] Stéphanie Pouzieux,[‡] Laure Delarbre,[‡] Sébastien Maignan,[‡] Thomas Bertrand,[‡] Kirsten Bjergarde,[#] Nina Ma,[#] Sylvette Lachaud,[†] Houlfa Guizani,[†] Rémi Lebel,[†] Gilles Doerflinger,[†] Sylvie Monget,[†] Sébastien Perron,[†] Francis Gasse,[†,×] Odile Angouillant-Boniface,[⊥] Bruno Filoche-Rommé,[†] Michel Murer,[⊥,×] Sylvie Gontier,[⊥,×] Céline Prévost,[⊥] Marie-Line Monteiro,[⊥] and Cécile Combeau[†]

[†]Oncology Drug Discovery, [‡]Structure Design Informatics, [§]Disposition Safety Animal Research, [∥]Chemical Development, and [⊥]Analytical Sciences, Sanofi, 13 Quai Jules Guesde, 94403 Vitry-sur-Seine, France

[#]Combinatorial Techno Center, Sanofi, 2090 East Innovation Park Drive, Oro Valley, Arizona 85755-1965, United States

Supporting Information

ABSTRACT: The Aurora family of serine/threonine kinases is essential for mitosis. Their crucial role in cell cycle regulation and aberrant expression in a broad range of malignancies have been demonstrated and have prompted intensive search for small molecule Aurora inhibitors. Indeed, over 10 of them have reached the clinic as potential anticancer therapies. We report herein the discovery and optimization of a novel series of tricyclic molecules that has led to SAR156497, an exquisitely selective Aurora A, B, and C inhibitor with in vitro and in vivo efficacy. We also provide insights into its mode of binding to its target proteins, which could explain its selectivity.

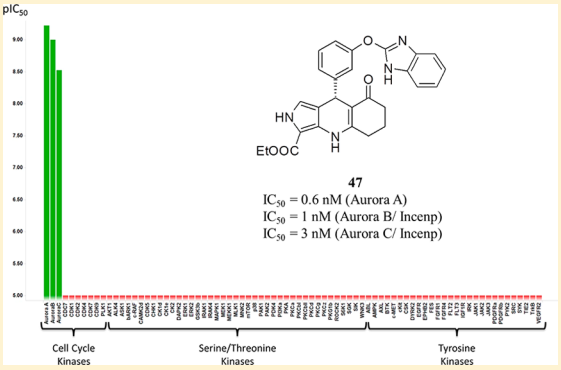

INTRODUCTION

The Aurora family (Aurora A, Aurora B, and Aurora C) belongs to the serine/threonine protein kinases.[1−6] The Aurora kinases all play a key role in cell division and are primarily active during mitosis. Although the three human Aurora kinases are highly homologous in sequence (particularly their ATP-binding sites), their respective functions during mitosis correlate with their distinct localization and expression in cells. Aurora A and Aurora B kinases are expressed in all dividing cells, whereas Aurora C kinase is mainly expressed in the testes and plays a role in spermatogenesis.[5] Aurora A is found at the centrosome in mitotic cells from late S and G2 phases until telophase but also localizes to the spindle throughout mitosis.[1] Functionally, Aurora A promotes centrosome maturation[1,2] and regulates the progression of mitosis by phosphorylation of multiple substrates.[1] Aurora B is localized at the centromeres in metaphase and remains associated with the spindle midzone during anaphase.[5] It is a chromosome passenger protein that regulates chromosome condensation (by phosphorylation of the chromatin protein histone H3), the spindle checkpoint, and cytokinesis.[3] Aurora C, whose functional role is less known, exhibits functions similar to those attributed to Aurora B and is required for cytokinesis.[4,5]

The Aurora kinases are aberrantly expressed in a variety of solid and liquid tumors. In addition, Aurora A and B overexpression has been associated with aneuploidy and poor prognosis in the case of ovarian carcinoma and non-small-cell lung cancer, respectively.[7] As a consequence, Aurora kinases have become attractive targets for new anticancer therapies[8,9] and in the past decade over 10 Aurora inhibitors have reached the clinic, the most advanced of them being alisertib (MLN8237, phase III),[8,10] ENMD-2076 (phase II),[8,11] and danusertib (phase II)[8,12] (Figure 1). Tozasertib,[8,13] the first one to enter the clinic, is a pan-Aurora inhibitor whose development was discontinued in phase II after the observation of QTc prolongation in one patient. Alisertib[8,10] is a potent Aurora A inhibitor also active on wild-type and T315I mutant bcr-abl, currently in a phase III clinical trial for the treatment of peripheral T-cell lymphoma. ENMD-2076[8,11] also inhibits Aurora A as well as kinases involved in angiogenesis (VEGFRs, FGFRs) and has received orphan drug designation from the U.S. Food and Drug Administration for the treatment of ovarian cancer, multiple myeloma, acute myeloid leukemia, and more recently hepatocellular carcinoma. Finally, danusertib[8,12] is a pan-Aurora kinase inhibitor with additional inhibitory activity on several receptor tyrosine kinases (i.e., wild-type and T315I mutant bcr-

Special Issue: New Frontiers in Kinases

Received: August 29, 2014

   dx.doi.org/10.1021/jm501326k | J. Med. Chem. XXXX, XXX, XXX−XXX

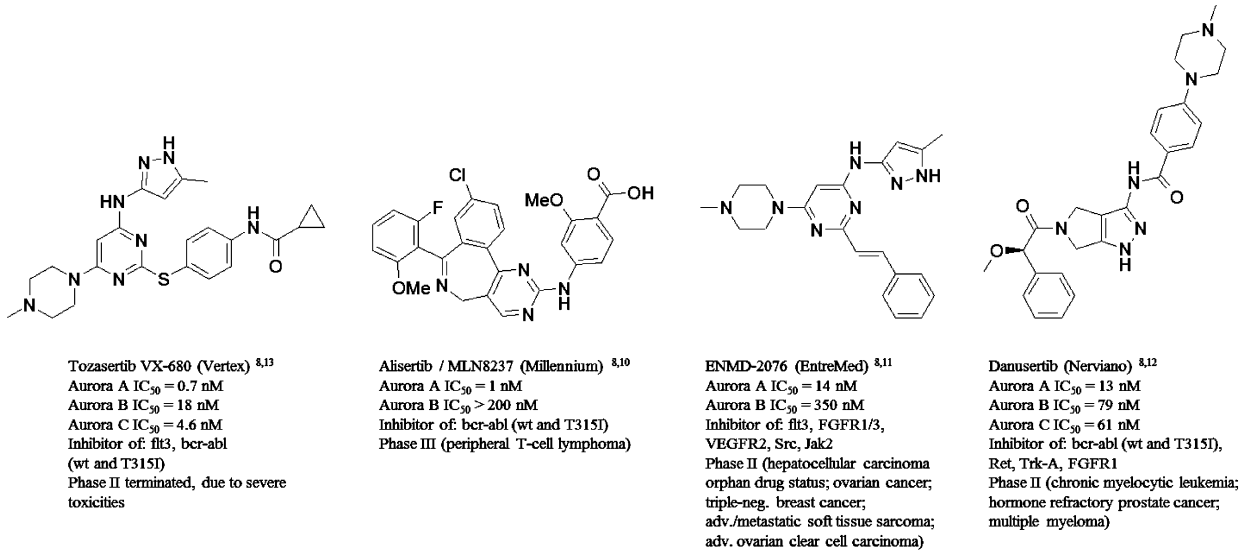

Figure 1. Some past and present Aurora inhibitors in advanced clinical trials.

abl, Ret, Trk-A, FGFR1) and is currently in phase II clinical trials for the treatment of a variety of solid and liquid malignancies.

This paper describes the discovery and optimization of a new series of tricyclic molecules[14] originating from virtual screening that have led to SAR156497, an exquisitely selective pan-Aurora inhibitor. Special emphasis in the optimization program has been put on improvement of metabolic stability, cytochrome P-450 3A4 inhibition, and selectivity versus PDE3. We also disclose the X-ray structure of SAR156497 bound to human Aurora A kinase domain at 3.2 Å resolution which provides insights into its mode of binding to its target proteins and could rationalize its selectivity versus other kinases. Finally, we provide in vitro and in vivo efficacy data on relevant tumor models.

LEAD DISCOVERY AND OPTIMIZATION

A virtual screening[15] was performed on the Sanofi combinatorial compound collection to identify potential Aurora inhibitors. Namely, a structure-based pharmacophore model was generated using four in-house X-ray structures of Aurora A bound to previously identified inhibitors from different chemical series (structures of three DFG-in inhibitors and one DFG-out inhibitor).[16,17] A six-point pharmacophore model was thus generated from the bound conformations (two aromatic features, one hydrophobic feature, one hydrogen-bond acceptor toward Ala213 in the hinge region, and two hydrogen-bond acceptors toward Glu211 and Ala213 in the hinge region) using Catalyst.[18] The 800 000 combinatorial compound collection was then screened using this pharmacophore model with a partial match option (i.e., at least three feature matches, with the hydrogen-bond acceptor to the hinge region as a mandatory match). Compounds passing this first step were then subjected to an ensemble docking using the four above-mentioned crystal structures of Aurora A with the GOLD[19] docking tool (with default precision settings and GoldScore as the scoring function), and the top six poses per each compound were saved. Then the top-ranked 20% compounds from GOLD docking were subjected to docking with GLIDE[20] (with Glidescore and in standard precision mode), saving again six top-ranked poses for each compound for further postprocessing. Finally, the postprocessing was performed by comparison of the GLIDE-docked poses with the probability statistics grid in the binding site of the crystal structures. Probability statistics for hydrophobic and hydrophilic regions within the binding site were calculated using the MOE[21] modeling software. Compounds that correctly matched the probability distribution (hydrophobic with hydrophobic, polar with polar, etc. and displaying no mismatches) were prioritized for in vitro screening. Chemotype diversity was also used as additional selection criteria. These efforts resulted in the selection of 3500 compounds that were screened in vitro on Aurora A at 10 μM concentration. Five active chemical series were identified, and 1,2,4,6,7,8-hexahydro-5*H*-pyrazolo[3,4-*b*]-[1,7]naphthyridin-5-ones rapidly emerged on the basis of selectivity data, with **1** as a prototype compound (Figure 2). The latter displayed an IC_{50} of 9.8 μM and was found selective (IC_{50} > 20 μM) vs a set of kinases including P-38, Fak, Tie2, and IGF1R.

A crystal structure of compound **1** in complex with Aurora A at 2.0 Å resolution (Figure 3) shows that the pyrazole A ring makes two direct H-bonds with the hinge region of Aurora A, namely, residues Glu211 and Ala213. The nitrogen atom of ring B is

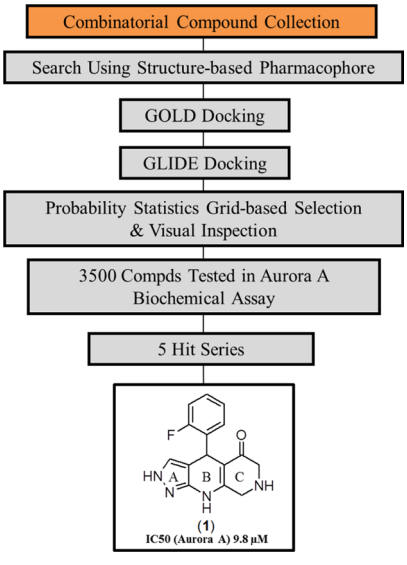

Figure 2. Virtual screening and hit identification process.

dx.doi.org/10.1021/jm501326k | J. Med. Chem. XXXX, XXX, XXX−XXX

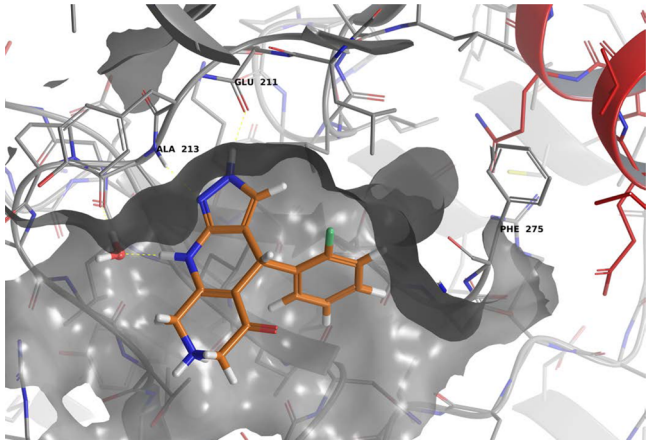

Figure 3. Crystal structure of (**1**) (orange) in complex with Aurora A (gray) at 2.0 Å resolution. Hydrogen bonds between (**1**) and the hinge region/water molecule are depicted as yellow dashed lines. Helix C is colored in red.

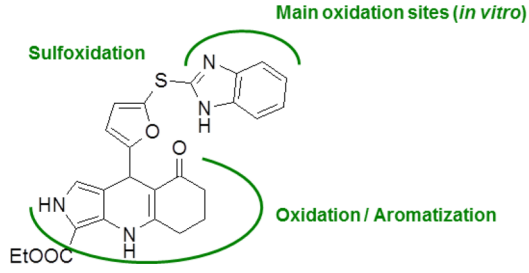

Figure 4. Metabolism map of compound **16**, based on mouse/rat/human hepatic microsomal fractions analysis.

involved in a water-mediated H-bond to the hinge with the carbonyl moiety of Ala213, and the phenyl substituent lies between the hydrophobic back pocket and the ribose pocket. The C ring occupies the ribose pocket partially and extends toward the solvent. Residues 276−292 from the activation loop are not observed in the electron density. Also, the conformation of the DFG motif[16] in this kinase complex adopts a position in between "in" and "out"[17] with the phenylalanine side chain of Phe275 oriented toward the N-lobe and in contact with the αC helix,[22a] the latter being shifted compared to a typical kinase active conformation.[22b] The protein conformation obtained in this complex is therefore clearly an inactive conformation of the kinase.[22c]

Thus, a potential strategy to improve the affinity of this series of inhibitors would be to extend toward the back pocket in order to increase the number of intermolecular interactions with nonconserved residues to maintain a good level of selectivity versus other kinases.

On the basis of these data, we first focused our hit exploration program on the improvement of Aurora A inhibition. Modification of the phenyl side chain could potentially improve affinity for the target protein, whereas the ring C nitrogen atom could serve as a handle to modulate ADME properties. All compounds were prepared as racemates to quickly establish preliminary SAR. Indeed, replacement of the phenyl moiety first by a phenoxyphenyl moiety and then by an (imidazol-2-ylsulfanyl)furan-2-yl side chain combined with replacement of the ring C nitrogen by a carbon atom resulted in improvement of potency by a factor 5 in the Aurora A kinase assay and provided for the first time a compound that inhibited cell proliferation

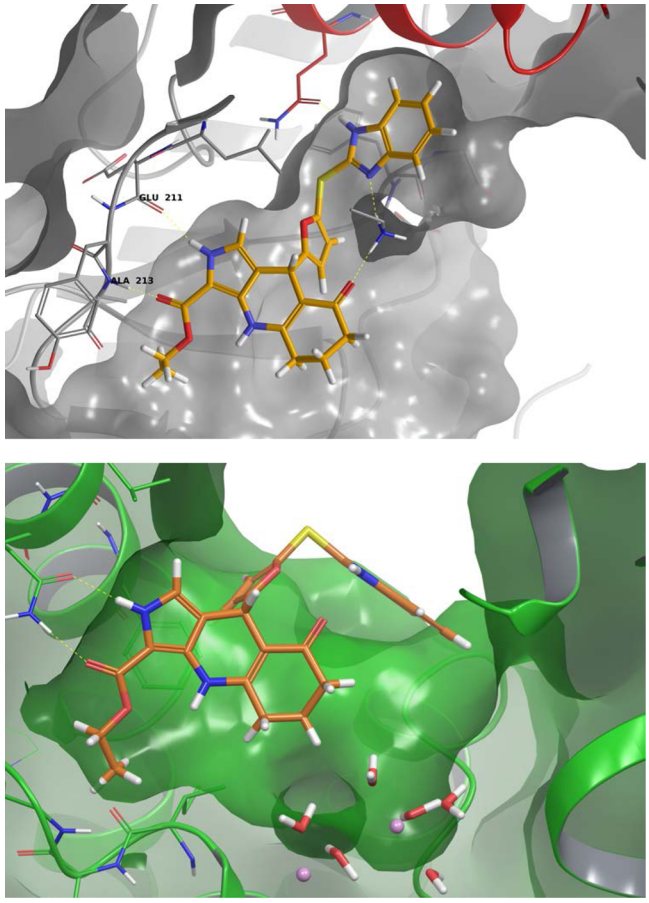

Figure 5. Top: X-ray structure of **16** (orange) bound to Aurora A (gray) at 1.9 Å resolution. Hydrogen bonds between **16** and Aurora A are depicted as yellow dashed lines. Helix C is colored in red. Bottom: Docking of **16** (orange) into the X-ray structure of PDE3B (green, PDB code 1SOJ). Taken together, these two binding modes highlight potential strategies to improve the selectivity of **16** on Aurora A vs PDE3, e.g., substitution on ring C, modification of ring A, or modification of the benzimidazole moiety.

(compound **8**: IC_{50} = 18 nM (Aurora A); IC_{50} = 300 nM (HeLa cell proliferation assay)) (Table 1).

Next, modification or replacement of the hinge-binding pyrazole ring A by various heterocycles was studied and the biochemical assay panel was extended to Aurora B (Table 2). Most of the time, the compounds displayed higher potency on Aurora B vs Aurora A; however, we observed that inhibition of cell proliferation correlated better with inhibition of Aurora A. Inversion of the nitrogen atoms position and substitution by a carboxylic acid derivative (compounds **8**−**11**) decreased potency on Aurora A and led to a loss of cellular activity. Moreover, replacement by a methyl thiophene-2-carboxylate resulted in no change in overall potency, whereas replacement by a pyrrole led to a decrease in biochemical and cellular potency (compounds **13** and **14**, respectively). Finally, encouraging results were obtained with potent 2-ethoxycarbonylpyrrole derivative **15**. The latter was resolved via chiral chromatography to obtain the corresponding pure enantiomers **16** and **17**. It is worth noting that **16** is over 125 times more potent than **17** on Aurora A and Aurora B and over 400 times more potent in the cell proliferation assay. Conversion of **16** into its methyl ester and acid derivatives (**18** and **19**, respectively) did not improve potency. Compound **16** was therefore considered as our lead compound (Table 2).

dx.doi.org/10.1021/jm501326k | J. Med. Chem. XXXX, XXX, XXX−XXX

Table 1. Biochemical and Cellular Activity of a Selection of Racemic 1,2,4,6,7,8-Hexahydro-5*H*-pyrazolo[3,4-*b*][1,7]naphthyridin-5-ones Modified on Rings B and C

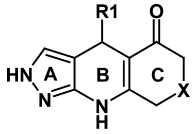

Cpd.	X	R1	Aurora A [a] IC_{50} (nM)	HeLa [b] IC_{50} (nM)	Ligand Efficiency Aurora A (Kcal/Mol)
1	NH		9800	>10000	0.33
2	NH	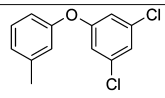	300	>10000	0.31
3	NH	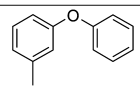	5082	>10000	0.27
4	NH	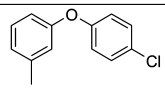	2739	>10000	0.27
5	NH	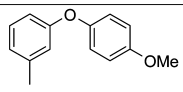	6288	>10000	0.25
6	NH	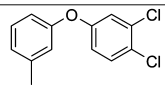	600	>10000	0.29
7	NH	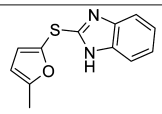	100	>10000	0.33
8	CH_2	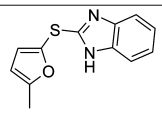	18	300	0.37

[a] IC_{50} values are reported as the mean from at least two independent experiments. See Supporting Information for assay details. [b] Proliferation inhibition in HeLa cell line. See Supporting Information for assay details.

To our delight, **16** combined high potency against Aurora kinases with unique selectivity against a panel of 64 kinases (Supporting Information, section S1; Table 1). However, despite high potency on Aurora A and Aurora B and antitumor efficacy when administered to immunocompromised mice bearing tumor xenografts, progression of compound **16** was hampered by low plasma exposure in rats, high clearance in human hepatocytes, and significant phosphodiesterase 3 (PDE3) inhibition (i.e., IC_{50} = 270 nM).[23] It is important to note that ester hydrolysis was never detected as a major metabolic pathway within this series (e.g., for compounds **16**, **20**, **33**, and **47**; data not shown) and that the ester moiety was revealed to be highly chemically stable, probably because of its vinylogous character.

Our lead optimization program was therefore focused on improving (i) metabolic stability, based on in vitro metabolism profiles obtained from mouse/rat/human hepatic microsomal fractions (Figure 4), and (ii) selectivity versus PDE3, based on a PDE3 model (Figures 5).

Table 2. Replacement of Pyrazole Ring A by Various Heterocycles

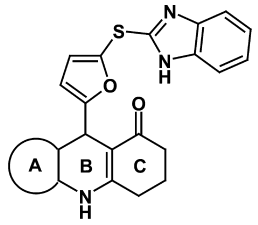

Cpd.	A	Optical purity	Aurora A [a] IC_{50} (nM)	Aurora B [a] IC_{50} (nM)	HeLa [b] IC_{50} (nM)	Ligand Efficiency Aurora A (Kcal/Mol)
8		(+/-)	18	5	300	0.37
9		(+/-)	>10000	500	>10000	<0.24
10		(+/-)	706	33	7700	0.25
11		(+/-)	2344	19	>10000	0.24
12		(+/-)	>10000	>10000	>10000	<0.21
13		(+/-)	11	5	127	0.33
14		(+)	377	127	3700	0.30
15		(+/-)	9	8	15	0.33
16		(+)	4	3	16	0.34
17		(-)	>500	>500	7000	<0.25
18		(+)	2	2	26	0.36
19		(+)	75	16	8751	0.31

[a] IC_{50} values are reported as the mean from at least two independent experiments. See Supporting Information for assay details. [b] Proliferation inhibition in HeLa cell line. See Supporting Information for assay details.

Thus, the different sites of the molecule that were modified in priority were the side chain to address metabolic stability on one hand and cycle A and cycle C (i.e., substitution) to address PDE3 inhibition on the other hand.

Metabolic stability and reversible and mechanism-based (MBI) cytochrome P-450 3A4 inhibition[24] data for a set of analogs that have been modified either on the side chain or at cycle C are reported in Table 3. Metabolic stability was recorded in human and mouse microsomes, respectively, and MBI was measured as negative slope (see Supporting Information for assay details). Compounds were tested most of the time as racemic mixtures; however, a few of them were selected for further profiling and were therefore tested as pure enantiomers.

dx.doi.org/10.1021/jm501326k | J. Med. Chem. XXXX, XXX, XXX−XXX

Table 3. CYP 3A4 Inhibition and Metabolic Stability for a Selection of Analogs

Cpd.	Structure	Optical purity	Aurora A [a] IC_{50} (nM)	Aurora B [a] IC_{50} (nM)	CyP 3A4 IC50 (μM)	CyP 3A4 [b] MBI (slope)	Metabolism human microsomes (%)	Metabolism mouse microsomes (%)
16	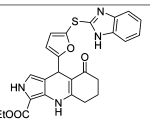	(+)	4	3	0.19	-2	69	83
20	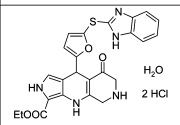	(+)	3	2	0.17	No MBI	66	60
21	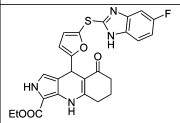	(+/-)	15	11	12	-13	73	77
22	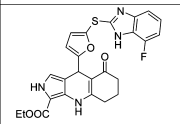	(+/-)	4	6	4.5	-12	47	58
23	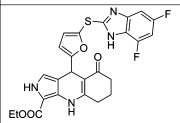	(+)	8	4	1	-10	66	36
24	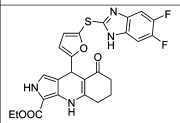	(+/-)	22	6	8.4	-11	58	55
25	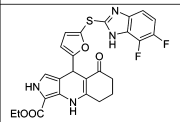	(+/-)	10	7	34	-12	66	66
26	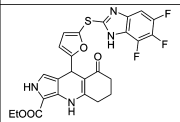	(+/-)	22	7	23	-10	46	22

Cpd.	Structure	Optical purity	Aurora A [a] IC_{50} (nM)	Aurora B [a] IC_{50} (nM)	CyP 3A4 IC50 (μM)	CyP 3A4 [b] MBI (slope)	Metabolism human microsomes (%)	Metabolism mouse microsomes (%)
27	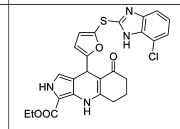	(+/-)	4	7	0.05	No MBI	68	85
28	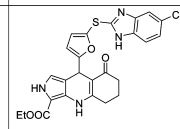	(+/-)	34	10	nd [c]	nd [c]	90	88
29	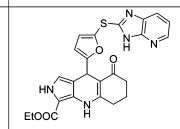	(+/-)	31	12	nd [c]	potent MBI	49	49
30	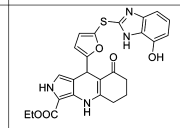	(+/-)	25	8	0.49	-3	40	37
31	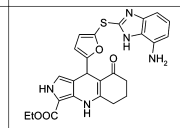	(+/-)	60	25	0.08	No MBI	23	35
32	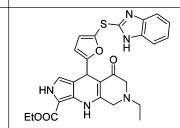	(+/-)	8	6	nd [c]	nd [c]	65	99
33	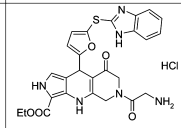	(+)	20	4	0.5	No MBI	65	30
34	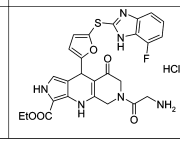	(+)	15	2	nd [c,d]	nd [c]	20	17

[a] IC_{50} values are reported as the mean from at least 2 independent experiments. See Supporting Information for assay details. [b] CYP 3A4 mechanism-based inhibition measured as negative slope. See Supporting Information for assay details. [c] nd: not determined. [d] A 2 μM IC_{50} on cytochrome P450 3A4 inhibition was measured in human liver microsome using midazolam as substrate. See Supporting Information for assay details.

Replacement of cyclohexenone cycle C by dehydropiperidinone (compound **20** vs **16**) had no effect either on CYP 3A4 inhibition or on metabolism. Introduction of fluorine atoms on the benzimidazole moiety (i.e., compounds **21**−**26**) decreased CYP 3A4 competitive inhibition but induced mechanism-based inhibition, as indicated by their corresponding highly negative slope values. In addition, fluorination of the benzimidazole moiety had little effect on metabolic stability in mice or human microsomes. Chlorination of the benzimidazole moiety (i.e., compounds **27** and **28**) did not improve metabolic stability and tended to decrease potency vs Aurora A, and it can be noticed that **27** is a potent and competitive CYP 3A4 inhibitor. The introduction of polarity in the benzimidazole moiety (**29**, **30**, and **31**) improved metabolic stability and decreased mechanism-based CYP 3A4 inhibition significantly; however, these compounds remained potent competitive CYP 3A4 inhibitors. The substitution of dehydropiperidinone cycle C tended to decrease metabolic stability (**32** vs **20**). Finally, glycine amide derivatives were prepared (i.e., **33** and **34**). The former (benzimidazole side chain) had a slightly improved metabolic stability vs its amine analog (**20**) and displayed some competitive inhibition of CYP 3A4, whereas its 7-fluorobenzimidazole analog (**34**) had a satisfactory (i.e., <40%) metabolic stability combined with moderate CYP 3A4 inhibition (this value was measured in different experimental conditions compared to the other compounds (Table 3)).

Selectivity data vs PDE3 for a set of analogs that have been modified either on the side chain or at cycle A or cycle C are reported in Table 4, using compound **16** as a reference. Substitution at position 7 of the benzimidazole moiety did not decrease PDE3 inhibition (entries 2−4 vs entry 1). However, modification of cycle A of the tricyclic moiety (i.e., replacement of the ethoxycarbonylpyrrole by a pyrazole (entry 5) or a thiophene (entry 6) or carboxylate modification (entry 7)) did modulate PDE3 inhibition, as compounds **8**, **13**, and **19** were less potent than compound **16**. Finally, although introduction of a nitrogen atom into cycle C of the tricyclic moiety did not influence PDE3 potency (entry 9), steric bulk on this nitrogen

dx.doi.org/10.1021/jm501326k | J. Med. Chem. XXXX, XXX, XXX−XXX

Table 4. Selectivity vs PDE3 for a Selection of Analogs

Entry	Cpd.	Structure	Optical purity	Aurora A [a] IC_{50} (nM)	Aurora B [a] IC_{50} (nM)	PDE3 [b] inhibition % @ 1 μM
1	16	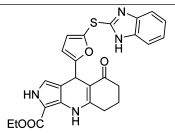	(+)	4	3	N/A [c]
2	35	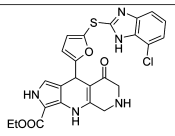	(+/-)	22	5	84
3	36	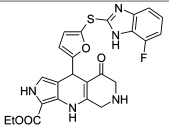	(+/-)	21	3	80
4	31	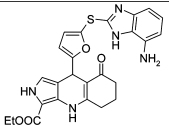	(+/-)	62	25	92
5	8	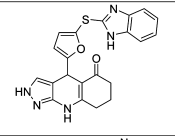	(+/-)	18	5	43
6	13	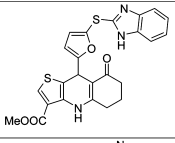	(+/-)	11	5	40
7	19	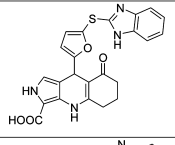	(+)	75	16	59
8	37	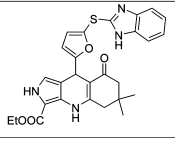	(+/-)	17	31	47
9	20	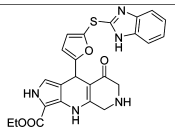	(+)	3	2	93
10	38	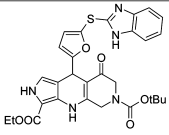	(+/-)	6	26	15
11	32	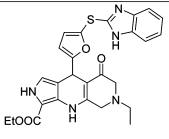	(+/-)	8	6	30
12	39	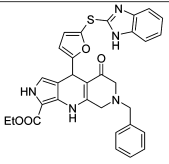	(+/-)	11	8	21
13	33	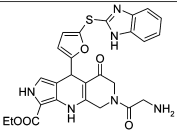	(+)	20	4	87
14	34	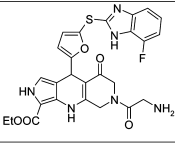	(+)	15	2	N/A [d]

[a] IC_{50} values are reported as the mean from at least two independent experiments. See Supporting Information for assay details. [b] See Supporting Information for assay details. [c] N/A: % inhibition not available. IC_{50} = 0.06 μM. [d] N/A: % inhibition not available. IC_{50} = 0.12 μM.

atom did decrease PDE3 inhibition significantly (entries 8 and 10−12) except for compounds **33** and **34** (entries 13−14) that have satisfactory metabolic stability and acceptable CYP 3A4 inhibition profiles (Table 3) but are unfortunately potent PDE3 inhibitors.

Thorough analysis of data from Tables 3 and 4 shows that it is difficult to combine an optimal ADME profile (high metabolic stability with no mechanism-based or competitive CYP 3A4 inhibition) and selectivity vs PDE3. This prompted us to step back and reconsider the results of Tables 1 and 2. We were encouraged to combine the phenoxyphenyl side chain that displayed low metabolization with the 8-oxo-4,5,6,7,8,9-hexahydro-2*H*-pyrrolo[3,4-*b*]quinoline-3-carboxylate scaffold that provided potent inhibition of Aurora A and Aurora B as well as proliferation of HeLa cells. Indeed, replacement of the furan ring of the (imidazol-2-ylsulfanyl)furan-2-yl side chain by a variety of five- and six-membered rings was carried out and the inhibitory potency was measured vs Aurora A and Aurora B and in the HeLa cell proliferation assay (Table 5). In the arylsulfanyl and heteroarylsulfanyl subseries, low potency in the cellular assay was observed (compounds **40**−**45**); however the 3-(1*H*-benzimidazol-2-yloxy)phenyl analogs (**46**, racemic; **47**, eutomer) of compound **16** displayed satisfactory potency in both the Aurora A/Aurora B and the cell proliferation assays.

To our satisfaction, compound **47** (SAR156497) combined high potency on all three isoforms of Aurora (i.e., IC_{50} = 0.6 nM (Aurora A), IC_{50} = 1 nM (Aurora B/Incenp), IC_{50} = 3 nM (Aurora C/Incenp) and ligand efficiency LE = 0.36 kCal/mol (Aurora A), LE = 0.35 kCal/mol (Aurora B/Incenp), LE = 0.33 kCal/mol (Aurora C/Incenp)) with an outstanding selectivity against a panel of over 110 kinases (Supporting Information, section S1; Table 2 and Figure 1). Furthermore, this compound represented the best compromise regarding the key issues of this chemical series (Supporting Information, section S3). Indeed, compound **47** displayed a 4 μM IC_{50} vs PDE3, a moderate metabolism in mice and human liver microsomes (53% and 32%, respectively), and only residual mechanism-based CYP 3A4 inhibition (k_{inact} = 0.076 min^{-1}, K_i = 0.99 μM measured with

dx.doi.org/10.1021/jm501326k | J. Med. Chem. XXXX, XXX, XXX−XXX

Table 5. Replacement of the Furan Ring of the (Imidazol-2-ylsulfanyl)furan-2-yl Side Chain

Cpd.	Structure	Optical purity	Aurora A [a] IC_{50} (nM)	Aurora B [a] IC_{50} (nM)	HeLa [b] IC_{50} (nM)
16	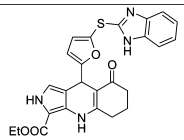	(+)	4	3	16
40	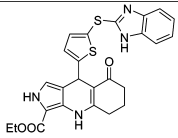	(+/-)	2300	180	4600
41	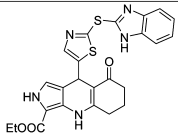	(+/-)	>10000	>10000	>10000
42	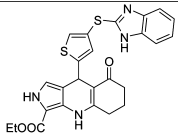	(+/-)	11	2	1500
43	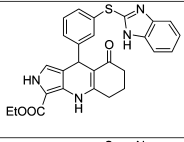	(+/-)	70	7	9700
44	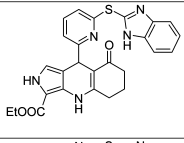	(+/-)	31	7	4400
45	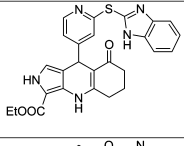	(+/-)	5200	1100	>10000
46	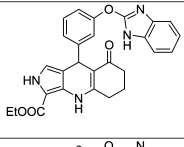	(+/-)	17	12	200
47	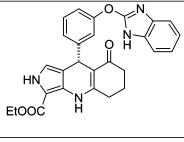	(-)	0.6	1	67

[a] IC_{50} values are reported as the mean from at least two independent experiments. See Supporting Information for assay details. [b] Proliferation inhibition in HeLa cell line. See Supporting Information for assay details.

recombinant human CYP 3A4 and midazolam as substrate; k_{inact} = 0.028 min^{-1}, K_i = 2.47 μM measured with human liver-derived CYP 3A4). Compound **47** was found to be active on a large panel of tumor cell lines (i.e., IC_{50} of 5−500 nM), induced polyploidy,[5] and inhibited the phophorylation of Aurora A and histone H3 (biomarkers of Aurora A and Aurora B, respectively)[5] in cultured tumor cells, as expected for an Aurora A and B inhibitor[2] (Supporting Information, section S2). In addition, it did not affect the viability of quiescent cells (PBMC, IC_{50} > 10 μM). The other properties of compound **47** are displayed in the Supporting Information, section S3. Compound **47** had an acceptable solubility at acidic pH and in pharmaceutical formulation, a good permeability in the Caco2 assay (P_{tot} = 60 nm/s) suggesting a suitable oral bioavailability, a satisfactory preliminary toxicological profile (no major sign of cardiotoxicity in dogs, negative in Ames and micronucleus assays), and a suitable pharmacokinetic profile (half-life of 2.4 h, distribution volume of 0.14 L/kg, and a 64% oral bioavailability in mice).

The structure of the complex of compound **47** bound to Aurora A was obtained by X-ray crystallography at 3.2 Å resolution (Figure 6). Residues 278−284 from the activation loop are not observed in the electron density. Two H-bonds are made with the hinge region of the kinase, namely, Glu211 with the pyrrole ring A and Ala213 with the ester moiety. A third H-bond is observed between the carbonyl moiety of ring C and Lys162, the latter forming a second H-bond with a nitrogen atom on the benzimidazole moiety of compound **47**. A fifth H-bond is finally made with the NH moiety of the benzimidazole and Gln185, on the αC Helix.[22a] The DFG motif displays here an "in" conformation,[16,17] and the overall kinase adopts an αC helix Glu-out inactivated conformation.[22] While other examples of kinase inhibitors stabilizing an inactivated conformation of their kinase target are known and have been described in the literature,[17] few of them exhibit as high a level of selectivity as this compound.[25] Besides, when Aurora kinases are compared with other members of the kinome, one residue making key interactions with compound **47** appears to be quite specific to Auroras: Gln185 (only found in Auroras, HUNK, and SGK494). This residue, which is either a leucine or a methionine in the vast majority of protein kinases, is located on the αC helix. It is part of the hydrophobic regulatory spine[26] and has been mentioned as a privileged residue for selectivity.[27] The stabilization of this inactivated conformation of Aurora A by compound **47**, with the αC helix shifted and stabilized by the benzimidazole moiety making an H-bond with the nonconserved residue Gln185, therefore provides a strong rationale for the high level of kinase selectivity observed with this compound.[5] On the other hand, it is worth noting that compound **47** is a pan-Aurora inhibitor. This lack of selectivity within the Aurora family is probably due to the fact that 94% of the 18 residues in direct interaction with compound **47** are conserved in all Aurora isoforms (the only

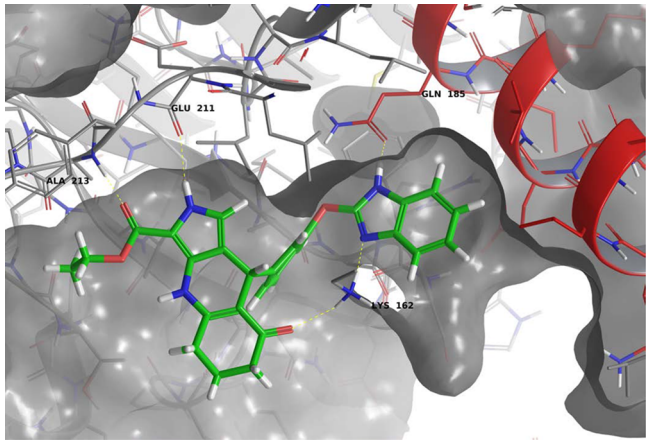

Figure 6. X-ray structure of compound **47** (green) bound to Aurora A (gray) at 3.2 Å resolution. Hydrogen bonds between **47** and Aurora A are depicted as yellow dashed lines. Helix C is colored in red.

dx.doi.org/10.1021/jm501326k | J. Med. Chem. XXXX, XXX, XXX−XXX

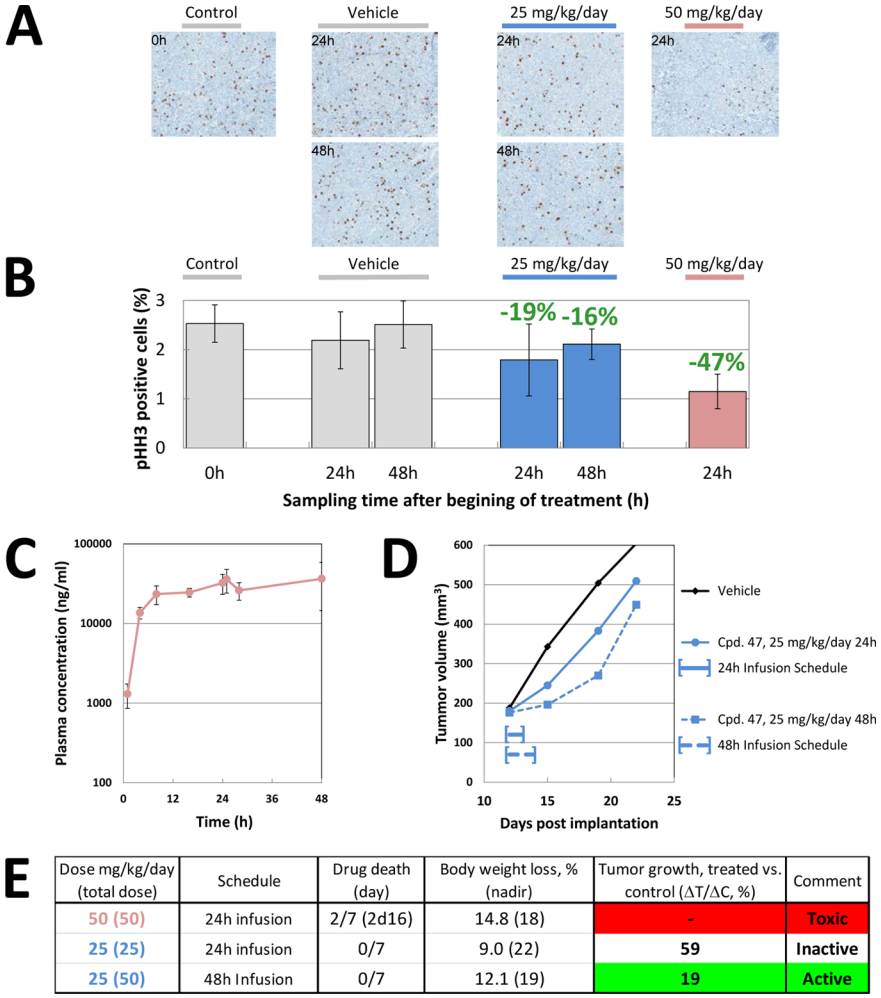

E

Dose mg/kg/day (total dose)	Schedule	Drug death (day)	Body weight loss, % (nadir)	Tumor growth, treated vs. control (ΔT/ΔC, %)	Comment
50 (50)	24h infusion	2/7 (2d16)	14.8 (18)	-	Toxic
25 (25)	24h infusion	0/7	9.0 (22)	59	Inactive
25 (50)	48h Infusion	0/7	12.1 (19)	19	Active

Figure 7. PK/PD and efficacy analysis of compound **47** in SCID female mice bearing human colon adenocarcinoma HCT116 xenografts. Compound **47** sulfate salt was administered subcutaneously in continuous infusion using ALZET micropump at an 8 μL/h flow rate for 24 or 48 h and at doses of 25 mg kg^{-1} day^{-1} (blue curves) and 50 mg kg^{-1} day^{-1} (pink curves). Pharmacodynamic profile: (A) immunohistochemical detection of phosphohistone H3 (pHH3) positive cells under different treatment modalities; (B) pHH3 biomarker modulation under compound **47** treatment. Pharmacokinetic profile: (C) plasma concentration of compound **47**, administered at a 50 mg kg^{-1} day^{-1} dose for 48 h. Efficacy study: (D) tumor growth in mice treated with compound **47** at a 25 mg kg^{-1} day^{-1} dose for 24 and 48 h; (E) tabulated results of compound **47** efficacy study.

Scheme 1. Synthesis of Compounds Bearing a 5-(1*H*-Benzimidazol-2-ylsulfanyl)furan-2-yl Side Chain[a]

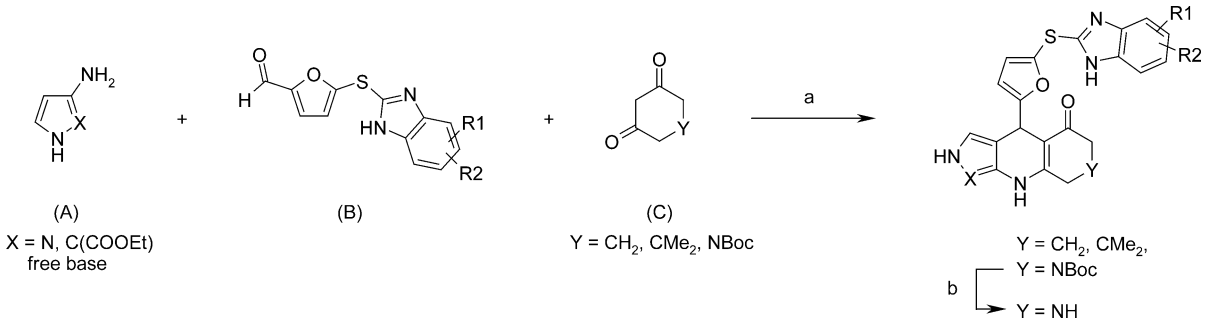

[a]Reagents and conditions: (a) EtOH or 1-butanol, reflux, 5−87%; (b) TFA, CH_2Cl_2 or 4 N HCl, dioxane.

nonconserved residue Val182 in Aurora A is an Ile in Aurora B and Aurora C). Nevertheless, the rationale for selective Aurora isoform inhibition vs pan-Aurora inhibition remains unclear and the ideal inhibitor profile has yet to be established.[5,28]

In Vivo Studies. Compound **47** was evaluated in different tumor models and showed significant efficacy in mice bearing the human acute myeloid leukemia EOL-1 and the human colon adenocarcinoma HCT116 xenografted subcutaneously (data not shown). To further characterize its antitumor efficacy, compound **47** was evaluated in PK/PD and efficacy studies in SCID female mice bearing human colon adenocarcinoma HCT116 xenografts (Figure 7). In this study compound **47** was administered in a continuous subcutaneous infusion with ALZET minipump for 24 or 48 h at a dose of 25 or 50 mg kg^{-1}

dx.doi.org/10.1021/jm501326k | J. Med. Chem. XXXX, XXX, XXX−XXX

Scheme 2. Synthesis of *N*-Alkyl and *N*-Acyl Derivatives[a]

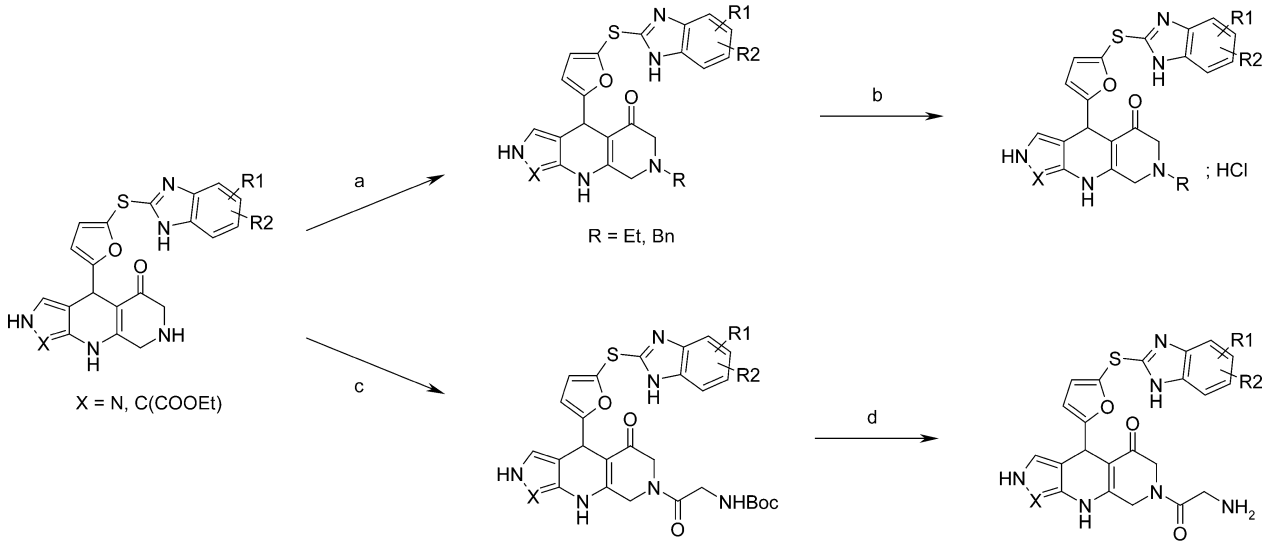

[a]Reagents and conditions: (a) R-I, *i*-Pr_2NEt, DMF, microwave, Δ; (b) 1 N HCl/Et_2O, EtOH, 0 °C; (c) Boc-Gly, HOBt/EDCI, CH_2Cl_2, 25 °C; (d) TFA, CH_2Cl_2 or 4 N HCl, dioxane.

day^{-1}. Pharmacokinetic analysis (Figure 7C) shows that at a dose of 50 mg kg^{-1} day^{-1}, a stable plasmatic concentration of ∼29 500 ng/mL (63 μM) was reached after 8 h and remained stable over the duration of the infusion. Pharmacodynamic analysis (Figure 7A and Figure 7B) shows that infusion at a 25 mg kg^{-1} day^{-1} dose induced a stable ∼20% decrease of phosphohistone H3 biomarker[2] for the duration of the treatment and that increasing the dose to 50 mg kg^{-1} day^{-1} resulted in ∼50% decrease of phosphohistone H3 positive cells. Regarding antitumor efficacy (Figure 7D and Figure 7E), the infusion of 25 mg kg^{-1} day^{-1} for 24 h was found inactive, the same dose showing a moderate activity after a 48 h infusion, while the superior dose of 50 mg kg^{-1} day^{-1} was found toxic after a 24 h infusion (i.e., body weight loss of >20%). These data indicate that compound **47** has a narrow therapeutic window in this model. Owing to its unique kinase selectivity, this narrow therapeutic window could probably be attributed to the pan-aurora profile of compound **47**.[1,2,8,12]

CHEMISTRY

The compounds were easily prepared via a Hantzsch-type[29] three-component reaction involving an arylamine, an aldehyde, and a cyclic 1,3-dione (Scheme 1). The reactions were run with equimolar quantities of each component in ethanol or 1-butanol at reflux to generate the target products in 5−87% yield.

When Y is a nitrogen atom, Boc-protected piperidine-3,5-dione[30] was used in the same conditions and the corresponding products were deprotected using trifluoroacetic acid in dichloromethane or 4 N hydrochloric acid in dioxane. Subsequent alkylation or acylation gave the desired tertiary amines and amides, respectively (Scheme 2).

Aldehydes (**B**) were prepared via a three-step synthetic route from commercially available *o*-nitroanilines. Reduction to the corresponding *o*-phenylenediamines followed by reaction with carbon disulfide, di-2-pyridylthionocarbonate, or 1,1′-thiocarbonyldiimidazole afforded the desired benzimidazolethiones. The latter reacted with 2-formyl-5-nitrofuran in the presence of sodium hydride to generate the desired aldehydes (**B**) (Scheme 3).

Scheme 3. Synthesis of Aldehydes (B)[a]

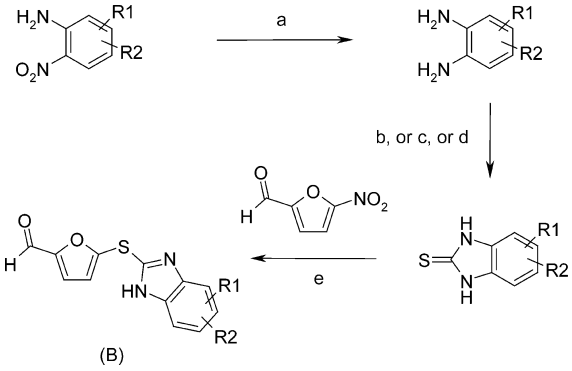

[a]Reagents and conditions: (a) $SnCl_2/NaBH_4$, AcOEt/*t*-BuOH, 60 °C; (b) CS_2, DMF, 25 °C; (c) di-2-pyridylthionocarbonate, THF, 25 °C; (d) 1,1′-thiocarbonyldiimidazole, THF, 25 °C; (e) NaH, THF.

Compound **47** was prepared according to a modified route (Scheme 4). Briefly, 2-chlorobenzimidazole was protected with a tetrahydropyranyl group and then reacted with 3-hydroxybenzaldehyde. The resulting aldehyde **50** was engaged in the three-component reaction in 1-butanol at reflux. Subsequent deprotection followed by resolution via chiral chromatography afforded the desired compound on multigram scale. Proof of absolute (*S*) configuration was obtained from the X-ray structure of **47** in complex with Aurora A (Figure 6).

CONCLUSION

We have discovered a novel series of highly potent tricyclic inhibitors of Aurora A, Aurora B and Aurora C with exquisite selectivity versus other kinases. These compounds were very easily prepared in one step via a Hantzsch-type three-component reaction involving an arylamine, an aldehyde, and a cyclic 1,3-dione. Optimization of their pharmacological properties has led to the identification of **47** (SAR156497) which represents the best compromise in this series from a multiparametric standpoint. Compound **47**, indeed combines high in vitro potency with satisfactory metabolic stability and limited CYP 3A4 and

dx.doi.org/10.1021/jm501326k | J. Med. Chem. XXXX, XXX, XXX−XXX

Scheme 4. Synthesis of 47 (SAR156497)[a]

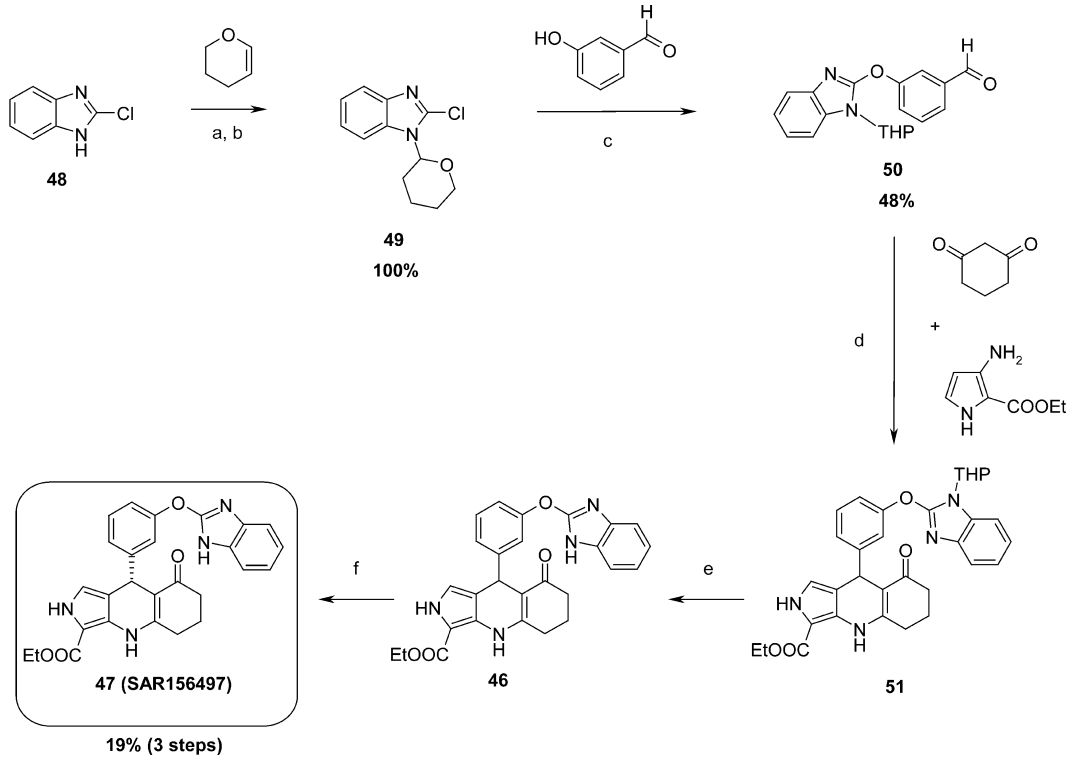

[a]Reagents and conditions: (a) cat. PTSA/THF, 50 °C; (b) MeONa, heptane, 12 °C to rt; (c) NaH, DMF, reflux; (d) 1-butanol, reflux, 30 min; (e) aq HCl, EtOH, rt; (f) chiral chromatography.

PDE3 inhibition. The X-ray structure of Aurora A bound to compound **47** provides insights into its unique kinase selectivity: the DFG motif of Aurora A displays an "in" conformation, and the protein adopts an αC helix Glu-out inactivated conformation. An amino acid located on the αC helix and quite specific to Aurora kinases (i.e., Gln185, only found in Auroras, HUNK, and SGK494) makes key interactions with compound **47** and could be the main determinant of this selectivity. In vitro, compound **47** displayed high antiproliferative activity on a large panel of tumor cell lines without correlation with any particular genetic signature or Aurora kinases expression. It induced significant modulation of Aurora A and Aurora B biomarkers (p-Aurora A and pHH3, respectively) and cell polyploidy, as expected from Aurora A/B inhibitors. In vivo efficacy has been demonstrated on relevant tumor models, but unfortunately, **47** displayed a narrow therapeutic window that we attribute to its pan-Aurora inhibitor profile.

EXPERIMENTAL METHODS

Chemistry. The nomenclature of the compounds was determined with the ACDLABS software, version 11.01. All solvents and reagents obtained from commercial sources were used without further purification. Thin layer chromatography was carried out on Merck silica gel 60 F254 glass plates. Flash chromatography was performed using prepacked Merck silica gel cartridges (15–40 μm). The microwave oven used was a Biotage Initiator 2.0, 400 W max, 2450 MHz instrument. The ^{1}H NMR spectra were performed on Bruker DPX-300, Bruker Avance DRX-400, and Bruker Avance DPX-500 spectrometers, respectively operating at 300, 400, and 500 MHz, with the chemical shifts (δ in ppm) in dimethylsulfoxide-d_6 (DMSO-d_6) referenced at 2.5 ppm at a temperature of 303 K and coupling constants (J) given in hertz. The optical rotations were recorded on a PerkinElmer 341 polarimeter.

The mass spectra were obtained by methods A–E:

Analytical LC/MS Method A. Analysis was conducted using Shimadzu LC-10AD HPLC pumps, a Gilson 215 well plate autosampler, and a Shimadzu SPD-10A UV detector. The mass spectrometer was a PE Sciex API 100LC instrument model with a YMC basic S5 column, with elution with a gradient of acetonitrile containing 0.1% TFA in water at a flow rate of 0.1 mL/min. Gradient details are given for each example. Compounds eluting off the column were detected by electrospray ionization mass spectrometry (EIMS).

Analytical LC/MS Method B. Analysis was conducted on a Waters model ZQ mass spectrometer working in positive and negative ion electrospray mode (mass range of 100–1200 amu) fitted on an Agilent HP1100 HPLC instrument. Separation was performed on a Waters Xbridge C18 column (3 mm × 50 mm, 2.5 μm particle diameter) maintained at a temperature of 60 °C and eluted by a gradient of acetronitrile in water containing 0.1% (v/v) formic acid at a flow rate of 1.1 mL/min. The gradient had the following characteristics: 5–100% acetonitrile in 5 min, plateau 100% acetonitrile for 0.5 min, then back to 5% acetonitrile in 1 min. Total run time was 7 min. In addition to mass spectrometry, UV diode array detection was performed at 210–400 nM wavelengths and evaporative light scattering was carried out using a Sedere Sedex 85 instrument.

Analytical LC/MS Method C. Analysis was conducted on a Waters model ZQ mass spectrometer working in positive and negative ion electrospray mode (mass range of 100–1200 amu) fitted on a Waters Acquity UPLC instrument. Separation was performed on a Waters UPLC BeH C18 column (2.1 mm × 50 mm, 1.7 μm particle diameter) maintained at a temperature of 55 °C, and elution was with a gradient of acetronitrile in water containing 0.1% (v/v) formic acid at a flow rate of 1.2 mL/min. The gradient had the following characteristics: 5–100% acetonitrile in 3 min, then back to 5% acetonitrile in 1 min. Total run time was 4.5 min. In addition to mass spectrometry, UV diode array detection was performed from 210 to 400 nm wavelengths.

Analytical LC/MS Method D. Analysis was conducted on an Acquity BEH C18 UPLC column, 1.7 μm, 2.1 mm × 50 mm (Waters) thermostated at 70 °C, with elution at a flow rate of 1 mL/min with a

dx.doi.org/10.1021/jm501326k | J. Med. Chem. XXXX, XXX, XXX–XXX

gradient from acetonitrile containing 0.1% formic acid (solvent B) into water containing 0.1% formic acid (solvent A). Elution program: isocratic stage at 5% of solvent B for 0.15 min, gradient from 5% to 100% of solvent B in 3.15 min, then return to the initial conditions over 0.1 min. The products were detected by an Acquity PDA diode array UV/vis detector (Waters, wavelength range scanned, 192−400 nm), a Sedex 85 light scattering detector (Sedere, nebulizing gas nitrogen, nebulizing temperature of 32 °C, nebulizing pressure 3.8 bar), and an Acquity SQD mass spectrometer (Waters, operating in positive and negative mode, mass range scanned: 80 to 800 amu).

Analytical LC/MS Method E. Analysis was conducted on a Waters UPLC-SQD instrument in positive and/or negative electrospray ionization mode (ES±), under the following liquid chromatography conditions. Column: ACQUITY BEH C18 1.7 μm, 2.1 mm × 50 mm; T_{column}, 50 °C; flow rate, 1 mL/min. Solvents: A, H_2O (0.1% formic acid); B, CH_3CN (0.1% formic acid). Gradient (2 min): 5−50% B in 0.8 min; 1.2 min, 100% B; 1.85 min, 100% B; 1.95 min, 5% B.

Preparative LC/MS Method A. Preparative LC/MS separations were carried out on Waters HPLC instruments: 515 HPLC pump; 2525 binary gradient module; 2487 DAD (dual absorbance detector); 2767 sample manager connected with a Micromass mass spectrometer. Products were separated on a YMC Combi Prep Pro C18 column, eluting with a gradient of acetonitrile containing 0.1% TFA in water containing 0.1% TFA at a flow rate of 32 mL/min. For each separation gradient programming was adapted on the basis of an analytical LC/MS chromatogram of the sample.

Preparative LC/MS Method B. Preparative LC/MS separations were carried out on a Waters FractionLynx system composed of a Waters model 600 gradient pump, a Waters model 515 regeneration pump, a Waters reagent manager make-up pump, a Waters model 2700 autoinjector, two Rheodyne model LabPro switches, a Waters model 996 photodiode array detector, a Waters model ZMD mass spectrometer, and a Gilson model 204 fraction collector. The instrument was controlled by a Waters FractionLynx software. At the output of the separating column the flow was split into a $^1/_{1000}$ ratio using a LC Packing AccuRate splitter; $^1/_{1000}$ of the flow was mixed with methanol (0.5 mL/min flow rate) and sent to the detectors. This flow was split again: $^3/_4$ of the flow was sent to the photodiode array detector and $^1/_4$ to the mass spectrometer. The rest of the output of the column ($^{999}/_{1000}$) was sent to the fraction collector where the flow was normally directed to waste unless the expected mass signal was detected by the FractionLynx software. The FractionLynx software was supplied with molecular formulas of expected compounds and triggered the collection of compounds when mass signals corresponding to $[M + H]^+$ and $[M + Na]^+$ were detected. In certain cases (depending on analytical LC/MS results, when $[M + 2H]^{2+}$ was detected as an intense ion) the FractionLynx software was additionally supplied with calculated half molecular weight (MW/2). In these conditions collection was also triggered when mass signals corresponding to $[M + 2H]^{2+}$ and $[M + Na + H]^{2+}$ were detected. Compounds were collected in glass tubes. After collection, solvent was evaporated in a Jouan model RC 10.10 centrifuge evaporator and the weight of compound was determined by weighing of the tubes after solvent evaporation. Column and gradient details are given for each example.

Purities of final compounds were measured by HPLC and/or LC/MS using UV detection at 220 nm and were ≥95.0%.

4-[3-(4-Chlorophenoxy)phenyl]-2,4,6,7,8,9-hexahydropyrazolo[3,4-9b]-1,7-naphthyridin-5-one, Trifluoroacetate (4). To a mixture of 107 mg of *N*-Boc-3,5-diketopiperidine (0.5 mmol) and 42 mg of 3-aminopyrazole (0.5 mmol) in 2.5 mL of ethanol was added 0.116 mL of 3-(4-chlorophenoxy)benzaldehyde (0.5 mmol). The mixture was heated at reflux temperature for $^1/_2$ h and cooled to rt. The solution was concentrated under vacuum. The resulting oily residue was dissolved in 2.5 mL of DCM and treated with 2.5 mL of TFA at rt for 1 h. After evaporation of the solvent, the crude product was directly purified via preparative LC/MS method A, resulting after lyophilization of the fractions in 70 mg (31%) of **4** as a white solid. Analytical LC/MS (method A): (2−85% ACN/H_2O gradient over 7 min) t_R = 3.91 min. EIMS $[M + H]^+$: m/z 393. ^{1}H NMR (300 MHz, DMSO-d_6): 3.70 (AB, 2H); 4.18 (AB, 2H); 5.17 (s, 1H); 6.65 (d, 1H); 6.94 (m, 4H); 7.22 (m, 1H); 7.45 (m, 3H); 9.80 (broad s, 2H); 10.4 (s, 1H).

4-[5-(1*H*-Benzimidazol-2-ylsulfanyl)furan-2-yl]-1,4,6,7,8,9-hexahydropyrazolo[3,4-9b]quinolin-5-one (8). To a mixture of 225 mg of 1,3-cyclohexanedione (2 mmol) and 183 mg of 3-aminopyrazole (2.2 mmol) in ethanol was added 490 mg of 5-(1*H*-benzimidazol-2-yl-sulfanyl)furan-2-carbaldehyde (2 mmol). The mixture was heated at reflux temperature for $^1/_2$ h and cooled to rt. The precipitate was collected by filtration and washed with ethanol to give 460 mg (58%) of **8** as a pale yellow solid. Analytical LC/MS (method A): (2−85% ACN/H_2O gradient over 7 min) t_R = 3.13 min. EIMS $[M + H]^+$: m/z 404. ^{1}H NMR (300 MHz, DMSO-d_6): 1.96 (m, 2H); 2.26 (m, 2H); 2.54 (m, 2H); 4.11 (s, 1H); 5.22 (s, 1H); 5.97 (s, 1H); 6.85 (s, 1H); 7.16 (m, 2H); 7.37 (m, 1H); 7.46 (s, 1H); 7.55 (m, 1H); 10.0 (s, 1H); 12.2 (s, 1H); 12.47 (s, 1H).

9-[5-(1*H*-Benzimidazol-2-ylsulfanyl)furan-2-yl]-8-oxo-4,5,6,7,8,9-hexahydro-2*H*-pyrrolo[3,4-*b*]quinoline-3-carboxylic Acid Ethyl Ester, Trifluoroacetate (15). 3-Amino-2-ethoxycarbonyl-pyrrole (31.5 g, 204 mmol), 5-(1*H*-benzimidazol-2-ylsulfanyl)furan-2-carbaldehyde (50 g, 204 mmol), and 1,3-cyclohexanedione (22.95 g 204 mmol) were combined in 2.5 L of 1-butanol, and the reaction mixture was heated at reflux temperature for 3 h and then concentrated under reduced pressure. The residue was resuspended in 1 L of ethanol and heated at reflux temperature for 2 h and allowed to cool to rt. The insoluble material was collected by filtration, washed with ethanol (0.4 L), diisopropyl ether (0.4 L), pentane (0.4 L), and dried under vacuum. The residue was resuspended in 2 L of acetonitrile, heated at reflux temperature for 2 h, and allowd to cool to rt. The insoluble material was collected by filtration, washed with acetonitrile (0.6 L), diisopropyl ether (0.6 L), pentane (0.6 L), and dried under vacuum to yield 41.5 g (43%) of **15** as a light gray powder. Analytical LC/MS (method B): t_R = 3.32 min. $[M + H]^+$: m/z 475.06. ^{1}H NMR (400 MHz, DMSO-d_6): 1.28 (t, J = 7.0 Hz, 3H); 1.88 (m, 2H); 2.25 (m, 2H); 2.58 (m, 1H); 2.79 (m, 1H); 4.26 (q, J = 7.0 Hz, 2H); 5.15 (s, 1H); 5.97 (d, J = 3.5 Hz, 1H); 6.79 (d, J = 3.5 Hz, 1H); 6.82 (d, J = 3.5 Hz, 1H); 7.12−7.17 (m, 2H); 7.47 (broad m, 2H); 8.40 (s, 1H); 11.4 (broad s, 1H); 12.4 (broad m, 1H).

(+)-9-[5-(1*H*-Benzimidazol-2-ylsulfanyl)furan-2-yl]-8-oxo-4,5,6,7,8,9-hexahydro-2*H*-pyrrolo[3,4-*b*]quinoline-3-carboxylic Acid Ethyl Ester (16) and (−)-9-[5-(1*H*-Benzimidazol-2-ylsulfanyl)furan-2-yl]-8-oxo-4,5,6,7,8,9-hexahydro-2*H*-pyrrolo-[3,4-*b*]quinoline-3-carboxylic Acid Ethyl Ester (17). Compound **15** (304 mg) was resolved via preparative chiral HPLC (column, Pirkle Whelk 01 SS 10 μm, 730 g, 360 mm × 60 mm; eluting solvent, *n*-heptane/ethanol 70/30 v/v + 0.1% diisopropylethylamine; rate, 90−125 mL/min; detection = 254 nm).

An amount of 118 mg (39%) of **16** was obtained as a yellow powder. Analytical LCMS (method A): $[M + H]^+$: m/z 475 (base peak). $[M - H]^-$: m/z 473 (base peak). Enantiomeric purity (chiral HPLC column, Pirkle Whelk 01 SS 10 μm, 250 mm × 4.6 mm; eluting solvent, *n*-heptane/ethanol 70/30 v/v + 0.1% diisopropylethylamine; rate, 1 mL/min; detection = 254 nm): >99%. $[\alpha]_D^{20}$ +192.8° ± 2.7 (c 0.36, CH_3OH).

An amount of 110 mg (36%) of **17** was obtained as a yellow powder. Analytical LCMS (method A): $[M + H]^+$: m/z 475 (base peak). $[M - H]^-$: m/z 473 (base peak). Enantiomeric purity: >98%. $[\alpha]_D^{20}$ −160.1° ± 2.1 (c 0.52, CH_3OH).

2-Chloro-1-(tetrahydropyran-2-yl)-1*H*-benzimidazole (49). A 10 L reactor was charged, under argon and with stirring, with 2.5 L of THF, 180 g of 2-chlorobenzimidazole (**48**, 1.18 mol), and 325 mL of 3,4-dihydro-2*H*-pyran (6.56 mol, 3 equiv). The reactor was heated until dissolution occurred (temperature of the mixture, 40 °C). Then an amount of 6.3 g of *p*-toluenesulfonic acid (0.033 mol, 0.028 equiv) was introduced. Heating was maintained between 49 and 52 °C for 2.5 h. After cooling to about 12 °C, an amount of 7.65 g of sodium methoxide (0.142 mol, 0.12 equiv) was added, with stirring maintained for a total time of 15 min. The temperature was then adjusted to 18 °C. An amount of 5 L of *n*-heptane was added, and the whole mixture was filtered on 300 g of Clarcel FLO-M, the solid being washed with 5 L of *n*-heptane. The filtrate was concentrated to dryness under reduced pressure to give 292.6 g (quantitative yield) of 2-chloro-1-(tetrahydropyran-2-yl)-1*H*-

dx.doi.org/10.1021/jm501326k | *J. Med. Chem.* XXXX, XXX, XXX−XXX

benzimidazole (**49**) in the form of a slightly yellow oil. ^{1}H NMR (400 MHz, DMSO-d_6): 1.42−2.01 (m, 5H); 2.21−2.34 (m, 1H); 3.69−3.78 (m, 1H); 4.12 (d, J = 11.4 Hz, 1H); 5.72 (dd, J = 2.4, 11.2 Hz, 1H); 7.22−7.34 (m, 2H); 7.62 (d, J = 7.2 Hz, 1H); 7.78 (d, J = 7.2 Hz, 1H).

3-[1-(Tetrahydropyran-2-yl)-1*H*-benzimidazol-2-yloxy]-benzaldehyde (50). Two 2 L three-necked round-bottom flasks, each equipped with a condenser, a thermometer, and a stirrer shaft, were charged under argon with *N*,*N*-dimethylformamide (0.4 L per flask) and 3-hydroxybenzaldehyde (68.5 g, flask 1; 64.2 g, flask 2; 1.08 mol). Sodium hydride (60% dispersion in mineral oil) was then added in portions (flask 1, 26 g; flask 2, 24 g; 1.25 mol, 1.2 equiv), the maximum temperature during the addition being 32 °C. 2-Chloro-1-(tetrahydropyran-2-yl)-1*H*-benzimidazole (**49**) (purity estimated at 85%) was then introduced (flask 1, 151 g in 0.5 L of DMF; flask 2, 142 g in 0.5 L of DMF; 1.05 mol, 0.97 equiv). The mixture was then heated at reflux (temperature 140 °C, temperature rise time 40 min), and the reflux was maintained for 1 h. Heating was then stopped, and the mixture was allowed to cool to rt over 1.5 h. The contents of the two flasks were combined, and the result was mixed slowly into 5 L of ice−water. The aqueous phase was then extracted with 4 × 2.5 L of AcOEt. The organic phases were combined, washed with 3 L of water and then with 2 L of saturated NaCl solution, and finally dried over $MgSO_4$ overnight. The organic phase was then filtered on a glass frit (porosity 4) and concentrated to dryness under reduced pressure to give 385 g of a brown oil. Analytical LC/MS (method D): t_R = 1.86 min. $[M + H]^+$: m/z 323.16.

A fraction of 158 g of the crude product obtained above was dissolved hot in 1.5 L of an *n*-heptane/AcOEt mixture (8:2 v/v), combined with 500 g of silica (70−30 mesh), and the mixture was stirred for 45 min. The resulting suspension was filtered on Celite and washed with 3 L of an *n*-heptane/AcOEt mixture (8:2 v/v). The organic phase was concentrated to dryness under reduced pressure. The residue was resuspended in 200 mL of isopropyl ether by mechanical stirring and ultrasound treatment and then filtered on a glass frit (porosity 3). The resulting solid was washed with 2 × 40 mL of isopropyl ether and dried under reduced pressure at 40 °C for 16 h to give 68 g of solid. A similar treatment was applied to the remainder of the crude product and produced 88 g of solid. The two solids were combined and homogenized to give 155.8 g (39%) of **50** in the form of pale beige crystals. Analytical LC/MS (method D): t_R=1.87 min. $[M + H]^+$: m/z 323.13. LC/MS (method E): t_R = 1.00 min. $[M + H]^+$: m/z 323. ^{1}H NMR (400 MHz, DMSO-d_6): 1.54−1.62 (m, 1H); 1.63−1.84 (m, 2H); 1.92−2.03 (m, 2H); 2.30−2.42 (m, 1H); 3.70−3.79 (m, 1H); 4.10 (d, J = 11.5 Hz, 1H); 5.74 (dd, J = 2.1, 11.1 Hz, 1H); 7.13−7.22 (m, 2H); 7.43 (d, J = 7.3 Hz, 1H); 7.65 (d, J = 7.3 Hz, 1H); 7.73 (t, J = 7.8 Hz, 1H); 7.78−7.83 (m, 1H); 7.87 (d, J = 7.8 Hz, 1H); 7.96 (s, 1H); 10.05 (s, 1H).

Ethyl 8-Oxo-9-{3-[1-(tetrahydro-pyran-2-yl)-1*H*-benzimidazol-2-yloxy]phenyl}-4,5,6,7,8,9-hexahydro-2*H*-pyrrolo[3,4-*b*]-quinoline-3-carboxylate (51). A 2 L conical flask was charged, under magnetic stirring, with 50 g (0.26 mol) of 3-amino-2-ethoxycarbonylpyrrole hydrochloride and 0.204 L (0.41 mol) of 2 N sodium hydroxide solution. The mixture was stirred for 15 min at rt and then extracted with 3 × 0.3 L of DCM. The organic phases were combined, dried over $MgSO_4$, and concentrated to dryness under reduced pressure. The residue was triturated with *n*-pentane, filtered, and dried under reduced pressure to a constant weight to give 36.4 g of crude 3-amino-2-ethoxycarbonylpyrrole as a brown solid. MS EI: m/z 154, $[M]^+$; m/z 126, $[M]^+ - C_2H_5$; m/z 108, $[M]^+ - OC_2H_5$ (base peak); m/z 80, 108 − CO.

A 2 L three-necked round-bottom flask equipped with a stirrer shaft, a thermometer, and a condenser was charged with 1.2 L of 1-butanol, 145 g of **50** (0.405 mol), 62.4 g of 3-amino-2-ethoxycarbonylpyrrole (1 equiv, 0.405 mol), 46.8 g of 1,3-cyclohexanedione (purity 97%) (1 equiv, 0.405 mol), and 70.5 mL of *N*,*N*-diisopropylethylamine (1 equiv), and the mixture was taken to reflux (temperature rise time 55 min, reflux maintained for 30 min, temperature 114 °C). The mixture was then cooled to rt and concentrated to dryness under reduced pressure to give 290 g of a brown oil containing **51**. Analytical LC/MS (method D): t_R = 1.96 min . $[M + H]^+$: m/z 553.35. A similar operation carried out with 35 g of **50** (0.098 mol) produced 72 g of a brown oil containing **51**. Analytical LC/MS (method D): t_R = 1.96 min . $[M + H]^+$: m/z 553.35.

Ethyl 8-Oxo-9-[3-(1*H*-benzimidazol-2-yloxy)phenyl]-4,5,6,7,8,9-hexahydro-2*H*-pyrrolo[3,4-*b*]quinoline-3-carboxylate (46). A 2 L round-bottomed flask was charged with 224 g of the brown oil containing **51**, 0.7 L of ethanol, and 0.243 L of 2 N hydrochloric acid. The mixture was stirred at rt for 16 h and then filtered on a glass frit (porosity 4). The filtrate was concentrated to dryness under reduced pressure, and the residue was triturated with 0.5 L of isopropyl ether. The solid was dried under reduced pressure at a constant weight to give 253 g of a brown solid containing **46**. Analytical LC/MS (method D): t_R = 1.46 min. $[M + H]^+$: m/z 469.29. A similar operation carried out with 54 g of the brown oil containing **51** produced 60 g of a brown solid containing **46**. Analytical LC/MS (method D): t_R = 1.48 min. $[M + H]^+$: m/z 469.29. An aliquot fraction of 0.8 g of the product obtained was purified by chromatography on a 50 g silica cartridge (10−90 μm) (Biotage SNAP, KP-Sil), eluting with an isocratic stage of DCM for 20 min, then a gradient from 0% to 1% by volume of isopropanol in dichloromethane over 1 h, and finally, an isocratic stage of dichloromethane/isopropanol (99:1 v/v) of 20 min. The fractions containing the expected product were combined to give 0.21 g of a yellow solid. The products of two similar chromatographic separations carried out on the same scale were crystallized from acetonitrile to give a total of 0.16 g of **46** in the form of beige crystals. Analytical LC/MS (method D): t_R = 1.61 min. $[M + H]^+$: m/z 469.28. ^{1}H NMR (400 MHz, DMSO-d_6): 1.29 (t, J = 7.0 Hz, 3H); 1.80−1.97 (m, 2H); 2.19−2.27 (m, 2H); 2.55−2.69 (m, 1H); 2.81 (dt, J = 4.8, 17.2 Hz, 1H); 4.26 (q, J = 7.0 Hz, 2H); 5.11 (s, 1H); 6.73 (d, J = 3.3 Hz, 1H); 7.02−7.16 (m, 5H); 7.25 (t, J = 7.9 Hz, 1H); 7.31−7.38 (m, 2H); 8.34 (s, 1H); 11.33 (broad s, 1H); 12.26 (broad s, 1H). Anal. Calcd for $C_{27}H_{24}N_4O_4$: C, 69.22; H, 5.16; N, 11.96; O, 13.66. Found: C, 68.72; H, 5.10; N, 11.82; H_2O, 0.38.

(−)-Ethyl 8-Oxo-9-[3-(1*H*-benzimidazol-2-yloxy)phenyl]-4,5,6,7,8,9-hexahydro-2*H*-pyrrolo[3,4-*b*]quinoline-3-carboxylate (47). The levorotatory enantiomer was purified from the crude product above on a Welk-01RR chiral column, 10 μm, 80 mm × 350 mm (Regis, USA), eluting with an *n*-heptane/dichloromethane/ethanol/triethylamine mixture (50/47.5/2.5/0.1 v/v/v/v). The elution of the products was detected by UV spectroscopy at 265 nm. Amounts of 10 g of the crude product described above were injected in each operation. Under these conditions, the peak corresponding to the levorotatory enantiomer was eluted with a t_R of 50−80 min. The fractions of purified levorotatory enantiomer corresponding to the operations needed to purify 310 g of the crude product described above were combined, homogenized, and concentrated to dryness under reduced pressure to give 50 g (19%) of **47** as a beige solid. Analytical LC/MS (method E): t_R = 0.77 min. $[M + H]^+$: m/z 469. $[M - H]^-$: m/z 467. ^{1}H NMR (400 MHz, DMSO-d_6): 1.29 (t, J = 7.1 Hz, 3H); 1.79−1.97 (m, 2H); 2.19−2.27 (m, 2H); 2.55−2.66 (m, 1H); 2.81 (dt, J = 4.9, 17.1 Hz, 1H); 4.26 (q, J = 7.1 Hz, 2H); 5.12 (s, 1H); 6.73 (d, J = 3.4 Hz, 1H); 7.02−7.16 (m, 5H); 7.25 (t, J = 8.3 Hz, 1H); 7.29−7.41 (m, 2H); 8.32 (s, 1H); 11.31 (broad s, 1H); 12.26 (broad s, 1H). IR, principal bands, cm^{-1}: 1678; 1578; 1525; 1442; 1188; 1043; 743. Optical rotation: $[\alpha]_D^{20}$ −38.6 ± 0.7 (c 0.070, CH_3OH). Anal. Calcd for $C_{27}H_{24}N_4O_4$: C, 69.22; H, 5.16; N, 11.96; O, 13.66. Found: C, 68.18; H, 5.92; N, 11.22; H_2O, 1.25.

■ ASSOCIATED CONTENT

Ⓢ Supporting Information

Selectivity data, cellular evaluation, and overall profile of compound **47** (SAR156497), full experimental synthetic procedures, protocols for in vitro and in vivo assays, and X-ray data collection and statistics. This material is available free of charge via the Internet at http://pubs.acs.org.

Accession Codes

Protein Data Bank codes are the following: compound **1**, 4UZH; compound **16**, 4UYN; compound **47**, 4UZD.

dx.doi.org/10.1021/jm501326k | J. Med. Chem. XXXX, XXX, XXX−XXX

AUTHOR INFORMATION

Corresponding Author

*E-mail: jean-christophe.carry@sanofi.com. Phone: +33(0)1 58 93 80 40. Fax: +33(0)1 58 93 80 14.

Present Addresses

[∞]R.L.M.: Cleave Biosciences, 866 Malcolm Road, Suite 100, Burlingame, CA 94010, U.S.

[×]F.G., M.M., and S.G. are currently retired from Sanofi.

Notes

The authors declare no competing financial interest.

ACKNOWLEDGMENTS

We thank Gary McCort for reviewing this manuscript. We also thank Dominique Gonnet and Frédéric Herman for their support in performing structural analyses. We thank Benoit Pasquier, Alan Binnie, and Anna Robinson for their contribution to in vitro pharmacology and Coumaran Egile for his contribution to in vivo pharmacology. We thank Francis Duffieux for his support in protein production. Finally, we thank Alessandra Bourgouin-Muller for her fine patent expertise.

ABBREVIATIONS USED

HLM, human liver microsome; MBI, mechanism based inhibition; PBMC, peripheral blood mononuclear cell; SCID, severe combined immunodeficiency

REFERENCES

(1) Goldenson, B.; Crispino, J. D. The Aurora Kinases in Cell Cycle and Leukemia. *Oncogene* [Online early access]. DOI: 10.1038/onc.2014.14. Published Online: March 17, **2014**.

(2) Kelly, K. R.; Ecsedy, J.; Devalingam, M.; Nawrocki, S. T.; Padmanabhan, S.; Giles, F. J.; Carew, J. S. Targeting Aurora Kinases in Cancer Treatment. *Curr. Drug Targets* **2011**, *12*, 2067−2078.

(3) Portella, G.; Passaro, C.; Chieffi, P. Aurora B: A New Prognostic Marker and Therapeutic Target in Cancer. *Curr. Med. Chem.* **2011**, *18*, 482−496.

(4) Kollareddy, M.; Dzubak, P.; Zheleva, D.; Hajduch, M. Aurora Kinases: Structure, Functions and Their Association with Cancer. *Biomed. Pap. Med. Fac. Univ. Palacky Olomouc Czech Repub.* **2008**, *152*, 27−33.

(5) Pollard, J. R.; Mortimore, M. Discovery and Development of Aurora Kinase Inhibitors as Anticancer Agents. *J. Med. Chem.* **2009**, *52*, 2629−2651.

(6) Gruneberg, U.; Neef, R.; Honda, R.; Nigg, E. A.; Barr, F. A. Relocation of Aurora B from Centromeres to the Central Spindle at the Metaphase to Anaphase Transition Requires MKlp2. *J. Cell Biol.* **2004**, *166*, 167−172.

(7) (a) Lassus, H.; Staff, S.; Leminen, A.; Isola, J.; Butzow, R. Aurora-A Overexpression and Aneuploidy Predict Poor Outcome in Serous Ovarian Carcinoma. *Gynecol. Oncol.* **2011**, *120*, 11−17. (b) Takeshita, M.; Koga, T.; Takayama, K.; Ijichi, K.; Yano, T.; Maehara, Y.; Nakanishi, Y.; Sueishi, K. Aurora-B Overexpression Is Correlated with Aneuploidy and Poor Prognosis in Non-Small Cell Lung Cancer. *Lung Cancer* **2013**, *80*, 85−90.

(8) Kollareddy, M.; Zheleva, D.; Dzubak, P.; Brahmkshatriya, P. S.; Lepsik, M.; Hajduch, M. Aurora Kinase Inhibitors: Progress toward the Clinic. *Invest. New Drugs* **2012**, *30*, 2411−2432.

(9) Green, M. R.; Woolery, J. E.; Mahadevan, D. Update on Aurora Kinase Targeted Therapeutics in Oncology. *Expert Opin. Drug Discovery* **2011**, *6*, 291−307.

(10) Görgün, G.; Hideshima, T.; Anderson, K. C. MLN-8237. *Drugs Future* **2010**, *35*, 903−908.

(11) (a) Zhang, S.; Farag, S. S. ENMD-2076. *Drugs Future* **2011**, *36*, 5−15. (b) How, J.; Yee, K.; Anderson, K. C. ENMD-2076 for Hematological Malignancies. *Expert. Opin. Invest. Drugs* **2012**, *21*, 717−732.

(12) Meulenbeld, H. J.; Mathijssen, R. H. J.; Verweij, J.; de Wit, R.; de Jonge, M. J. A. Danusertib, an Aurora Kinase Inhibitor. *Expert. Opin. Invest. Drugs* **2012**, *21*, 383−393.

(13) Wang, Y.; Serradell, N. VX-680/MK-0457. *Drugs Future* **2007**, *32*, 144−147.

(14) (a) Mauger, J.; Nair, A.; Ma, N.; Bjergarde, K.; Filoche-Rommé, B.; Angouillant-Boniface, O.; Mignani, S. Preparation of 1,4-Dihydropyridine-Fused Heterocycles as Inhibitors of Aurora Kinase. Eur. Pat. Appl. EP1746097A1 20070124, 2007. (b) Carry, J.-C.; Cheve, M.; Clerc, F.; Combeau, C.; Gontier, S.; Krick, A.; Lachaud, S.; Schio, L. Preparation of Benzimidazolylpyrrole Quinoline Derivatives as Anticancer Agents. PCT Int. Appl. WO2010133794A1 20101125, 2010. (c) Arokiassamy, N.; Billot, P.; Carry, J.-C.; Clavieres, P.; Clerc, F.; Crocq-Stuerga, V.; Lachaud, S.; Lienard, P.; Menegotto, J.; Schio, L. (−)-Ethyl 8-Oxo-9-[3-[(1*H*-benzimidazol-2-yl)oxy]phenyl]-4,5,6,7,8,9-hexahydro-2*H*-pyrrolo[3,4-*b*]quinoline-3-carboxylate, and Its Salt, Crystalline Form, Cocrystal, Processes for Preparation, Formulations, Pharmaceutical Compositions and New Use Particularly as Selective Inhibitors of Aurora Kinases for Treating Cancers. PCT Int. Appl. WO2012066486A1 20120524, 2012.

(15) (a) Sotriffer, C.; Klebe, G.; Stahl, M.; Böhm, H.-J. Docking and Scoring Functions/Virtual Screening. In *Burger's Medicinal Chemistry and Drug Discovery*, 6th ed.; Abraham, D. J., Ed.; Wiley: Hoboken, NJ, 2003; pp 281−331. (b) Kong, X.; Qin, J.; Li, Z.; Vultur, A.; Tong, L.; Feng, E.; Rajan, G.; Liu, S.; Lu, J.; Liang, Z.; Zheng, M.; Zhu, W.; Jiang, H.; Herlyn, M.; Liu, H.; Marmorstein, R.; Luo, C. Development of a Novel Class of B-Raf ^{V600E}-Selective Inhibitors through Virtual Screening and Hierarchical Hit Optimization. *Org. Biomol. Chem.* **2012**, *10*, 7402−7417.

(16) Kornev, A. P.; Haste, N. M.; Taylor, S. S.; Ten Eyck, L. F. Surface Comparison of Active and Inactive Protein Kinases Identifies a Conserved Activation Mechanism. *Proc.Natl. Acad. Sci. U.S.A.* **2006**, *103*, 17783−17788.

(17) Martin, M. P.; Zhu, J.-Y.; Lawrence, H. R.; Pireddu, R.; Luo, Y.; Alam, R.; Ozcan, S.; Sebti, S. M.; Lawrence, N. J.; Schönbrunn, E. A Novel Mechanism by Which Small Molecule Inhibitors Induce the DFG Flip in Aurora A. *ACS Chem. Biol.* **2012**, *7*, 698−706.

(18) *Catalyst*; Accelrys Software Inc.: San Diego, CA.

(19) (a) Jones, G.; Willett, P.; Glen, R. C. Molecular Recognition of Receptor Sites Using a Genetic Algorithm with a Description of Desolvation. *J. Mol. Biol.* **1995**, *245*, 43−53. (b) Jones, G.; Willett, P.; Glen, R. C.; Leach, A. R.; Taylor, R. Development and Validation of a Genetic Algorithm for Flexible Docking. *J. Mol. Biol.* **1997**, *267*, 727−748.

(20) (a) Friesner, R. A.; Banks, J. L.; Murphy, R. B.; Halgren, T. A.; Klicic, J. J.; Mainz, D. T.; Repasky, M. P.; Knoll, E. H.; Shelley, M.; Perry, J. K.; Shaw, D. E.; Francis, P.; Shenkin, P. S. Glide: A New Approach for Rapid, Accurate Docking and Scoring. 1. Method and Assessment of Docking Accuracy. *J. Med. Chem.* **2004**, *47*, 1739−1749. (b) Halgren, T. A.; Murphy, R. B.; Friesner, R. A.; Beard, H. S.; Frye, L. L.; Pollard, W. T.; Banks, J. L. Glide: A New Approach for Rapid, Accurate Docking and Scoring. 2. Enrichment Factors in Database Screening. *J. Med. Chem.* **2004**, *47*, 1750−1759.

(21) *Molecular Operating Environment (MOE)*; Chemical Computing Group Inc.: Montreal, Quebec, Canada.

(22) (a) Palmieri, L.; Rastelli, G. αC Helix Displacement as a General Approach for Allosteric Modulation of Protein Kinases. *Drug Discovery Today* **2013**, *18*, 407−414. (b) Zuccotto, F.; Ardini, E.; Casale, E.; Angiolini, M. Through the "Gatekeeper Door": Exploiting the Active Kinase Conformation. *J. Med. Chem.* **2010**, *53*, 2681−2694. (c) Alton, G. R.; Lunney, E. A. Targeting the Unactivated Conformations of Protein Kinases for Small Molecule Drug Discovery. *Expert Opin. Drug Discovery* **2008**, *3*, 595−605.

(23) (a) Zhang, J.; Herman, E. H.; Knapton, A.; Chadwick, D. P.; Whitehurst, V. E.; Koerner, J. E.; Papoian, T.; Ferrans, V. J.; Sistare, F. D. SK&F 95654-Induced Acute Cardiovascular Toxicity in Sprague−Dawley Rats—Histopathologic, Electron Microscopic, and Immuno-

histochemical Studies. *Toxicol. Pathol.* **2002**, *30*, 28−40. (b) Fossa, P.; Giordanetto, F.; Menozzi, G.; Mostia, L. Structural Basis for Selective PDE 3 Inhibition: A Docking Study. *Quant. Struct.−Act. Relat.* **2002**, *21*, 267−275.

(24) Zhou, S.; Chan, S. Y.; Goh, B. C.; Chan, E.; Duan, W.; Huang, M.; McLeod, H. L. Mechanism-Based Inhibition of Cytochrome P450 3A4 by Therapeutic Drugs. *Clin. Pharmacokinet.* **2005**, *44*, 279−304.

(25) Hu, Y.; Furtmann, N.; Bajorath, J. Current Compound Coverage of the Kinome *J. Med. Chem.* [Online early access]. DOI: 10.1021/jm5008159. Published Online: July 22, **2014**.

(26) Kornev, A. P.; Taylor, S. S. Defining the Conserved Internal Architecture of a Protein Kinase. *Biochim. Biophys. Acta, Proteins Proteomics* **2010**, *1804*, 440−444.

(27) Martin, E.; Mukherjee, P. Kinase-Kernel Models: Accurate in silico Screening of 4 Million Compounds across the Entire Human Kinome. *J. Chem. Inf. Model.* **2012**, *52*, 156−170.

(28) Bavetsias, V.; Faisal, A.; Crumpler, S.; Brown, N.; Kosmopoulou, M.; Joshi, A.; Atrash, B.; Pérez-Fuertes, Y.; Schmitt, J. A.; Boxall, K. J.; Burke, R.; Sun, C.; Avery, S.; Bush, K.; Henley, A.; Raynaud, F. I.; Workman, P.; Bayliss, R.; Linardopoulos, S.; Blagg, J. Aurora Isoform Selectivity: Design and Synthesis of Imidazo[4,5-*b*]pyridine Derivatives as Highly Selective Inhibitors of Aurora-A Kinase in Cells. *J. Med. Chem.* **2013**, *56*, 9122−9135.

(29) (a) Chebanov, V. A.; Saraev, V. E.; Desenko, S. M.; Chernenko, V. N.; Knyazeva, I. V.; Groth, U.; Glasnov, T. N.; Kappe, C. O. Tuning of Chemo- and Regioselectivities in Multicomponent Condensations of 5-Aminopyrazoles, Dimedone, and Aldehydes. *J. Org. Chem.* **2008**, *73*, 5110−5118. (b) Chebanov, V. A.; Saraev, V. E.; Desenko, S. M.; Chernenko, V. N.; Shishkina, S. V.; Shishkin, O. V.; Kobzar, K. M.; Kappe, C. O. One-Pot, Multicomponent Route to Pyrazoloquinolizinones. *Org. Lett.* **2007**, *9*, 1691−1694. (c) Drizin, I.; Altenbach, R. J.; Buckner, S. A.; Whiteaker, K. L.; Scott, V. E.; Darbyshire, J. F.; Jayanti, V.; Henry, R. F.; Coghlan, M. J.; Gopalakrishnan, M.; Carroll, W. A. Structure−Activity Studies for a Novel Series of Tricyclic Dihydropyridopyrazolones and Dihydropyridoisoxazolones as K_{ATP} Channel Openers. *Bioorg. Med. Chem.* **2004**, *12*, 1895−1904. (d) Quiroga, J.; Mejía, D.; Insuasty, B.; Abonía, R.; Nogueras, M.; Sánchez, A.; Cobo, J.; Low, J. N. Regioselective Synthesis of 4,7,8,9-Tetrahydro-2*H*-pyrazolo-[3,4-*b*]-quinolin-5(6*H*)-ones. Mechanism and Structural Analysis. *Tetrahedron* **2001**, *57*, 6947−6953.

(30) Knudsen, S. M.; Pettersson, I.; Lau, J.; Behrens, C.; Petersen, A. K.; Lau, J.; Garibay, P. W. Condensed Thiophene Derivatives and Their Use as Cyclic GLP-1 Agonists. PCT Int. Appl. WO2006003096, 2006.